EAI Endorsed Transactions
on Energy Web

Research Article **EAI.EU**

CNN-Attention-Based Renewable Energy Generation and Load Forecasting Method for Stable Operation of Smart Grids

Wei Luo[1, *]

[1] Nanjing University of Science and Technology Zijin College, China

Abstract

High renewable penetration increases source-load uncertainty and challenges the stable operation of smart grids. This paper proposes a prediction-driven framework that integrates CNN-Attention-based joint renewable generation and load forecasting with rolling optimization of a battery–supercapacitor hybrid energy storage system. The main innovation lies in coupling source-load forecasting with hybrid energy storage dispatch, so that predicted renewable generation and load trajectories can directly support rolling scheduling decisions. Multi-source temporal inputs, including wind power, photovoltaic power, load demand, meteorological variables, electricity price, and periodic time encodings, are used to characterize source-load coupling. One-dimensional convolution extracts local fluctuation features, while temporal attention assigns adaptive weights to informative historical periods. In the dispatch stage, the battery mainly undertakes low-frequency energy balancing, whereas the supercapacitor suppresses high-frequency power fluctuations. The optimization objective jointly considers grid purchase cost, storage degradation cost, renewable curtailment penalty, load shedding penalty, and grid power fluctuation penalty. Experiments were conducted on one-year operational data from a regional wind–photovoltaic–storage microgrid, with a 15-min sampling interval and 35,040 time steps. Compared with LSTM, GRU, CNN, CNN-LSTM, and Transformer baselines, the proposed model achieved the lowest forecasting errors, with MAE/RMSE/MAPE of 6.692 kW/8.322 kW/3.288% for renewable generation and 3.747 kW/4.490 kW/0.406% for load forecasting. At the dispatch level, the proposed strategy reduced the total operating cost index to 360, decreased grid power fluctuation to 3.4%, improved renewable accommodation to 90.6%, and lowered curtailment to 2.8%.

Keywords: smart grid; renewable energy forecasting; load forecasting; CNN-Attention; hybrid energy storage; rolling optimization; grid stability

Received on 30 May 2026, accepted on 28 July 2026, published on 13 August 2026

doi: 10.4108/ew.13260

1. Introduction

With the continuing transition toward low-carbon and intelligent energy systems, the penetration of wind power, photovoltaic generation, and other renewable energy sources in power systems has increased rapidly. Renewable energy output is strongly affected by meteorological factors such as wind speed, solar irradiance, temperature, humidity, and cloud cover, and therefore exhibits evident randomness, intermittency, and volatility [1,2]. Meanwhile, user-side load demand is influenced by temporal consumption patterns, weather conditions, electricity pricing mechanisms, and user behavior, resulting in considerable uncertainty [3,4]. The superposition of source-side and load-side uncertainties makes power balance, economic dispatch, renewable energy accommodation, and grid-connected power stability more difficult to maintain in smart grids with high renewable energy penetration.

Short-term renewable generation forecasting and load forecasting are fundamental tasks for smart grid energy management. In recent years, deep learning methods have been widely applied to wind power forecasting, photovoltaic forecasting, and short-term load forecasting because of their strong nonlinear representation ability [5,6]. Recurrent neural networks, such as long short-term memory networks and gated recurrent units, are effective in modeling temporal dependence. Convolutional neural networks can extract local fluctuation patterns from time-series data, while attention mechanisms and Transformer-based models can enhance the representation of key historical periods and long-range

Corresponding author. Email: luowei995@njust.edu.cn

temporal dependencies [7,8]. However, in high-renewable smart grid operation, renewable generation and load demand should not be regarded as two completely independent forecasting objects. Their combined effect determines the future net load trajectory, which further affects storage charging and discharging, grid interaction power, renewable curtailment, and load shedding risk. Therefore, forecasting models need to characterize source-load coupling rather than only reducing the prediction error of a single variable.

Energy storage systems play an important role in mitigating renewable energy fluctuations and improving grid flexibility. Battery energy storage has high energy density and is suitable for peak shaving, valley filling, and cross-period energy transfer. However, frequent charging and discharging may accelerate battery degradation and shorten service life [9]. Supercapacitors have high power density and fast response capability, making them suitable for suppressing short-term power shocks, although their energy capacity is limited. A battery–supercapacitor hybrid energy storage system can combine the advantages of energy-type storage and power-type storage. The battery mainly undertakes low-frequency energy balancing, while the supercapacitor responds to high-frequency power fluctuation, thereby improving renewable energy smoothing, grid stability support, and storage lifetime protection [10]. Recent studies on battery state estimation, neural-network-based state of energy estimation, and electrochemical-thermal modeling also indicate that more accurate state modeling and adaptive optimization are important for improving the reliability of storage-assisted smart grid operation.

Dispatch strategies also strongly affect smart grid operation. Rule-based control and fixed-threshold methods are simple but have limited adaptability to rapid renewable fluctuations and sudden load changes. Day-ahead optimization provides a global scheduling plan, but its response to real-time forecasting errors and short-term disturbances is insufficient. Model predictive control and rolling optimization update control commands within a finite prediction horizon according to the latest operating states, making them suitable for microgrid energy management and real-time optimization [11,12]. Therefore, integrating source-load forecasting with hybrid energy storage rolling optimization can establish a closed-loop process of forecasting, optimization, execution, and feedback, improving economy, renewable energy accommodation, and grid stability under uncertain conditions.

Although considerable progress has been made in renewable energy forecasting, load forecasting, energy storage control, and microgrid dispatch optimization, several limitations remain. First, many existing studies treat renewable generation forecasting and load forecasting as separate tasks, which may overlook the coupling among renewable output, load demand, meteorological variables, electricity price, and temporal factors. This limits the ability of forecasting results to reflect future net load variations and weakens storage dispatch coordination. Second, most deep learning forecasting models mainly focus on statistical prediction errors, while their connection with downstream dispatch decisions remains insufficient. In practical smart grid energy management, forecasting results should directly support storage charging and discharging, grid interaction control, and renewable energy accommodation. Third, conventional storage control strategies often fail to distinguish between low-frequency energy balancing and high-frequency fluctuation suppression, causing the battery to respond to frequent short-term disturbances. Finally, day-ahead or open-loop optimization methods cannot continuously incorporate updated source-load forecasts, storage state of charge, and grid power feedback, which limits their robustness under strong renewable fluctuations and forecasting errors [13,14].

To address these limitations, this paper proposes a prediction-driven CNN-Attention-based joint renewable generation and load forecasting method combined with battery–supercapacitor hybrid energy storage rolling optimization for stable smart grid operation [15]. Compared with conventional separate forecasting and independent dispatch methods, the main improvements of this study are as follows. First, a multi-source temporal feature system is constructed by integrating historical wind power, photovoltaic power, load power, meteorological variables, electricity price signals, and periodic time encodings, so that the dynamic coupling between renewable generation and load demand can be better characterized. Second, a convolutional neural network-attention (CNN-Attention) joint forecasting model is developed. One-dimensional convolution is used to extract local temporal fluctuation features, and temporal attention is introduced to assign adaptive weights to key historical periods that are more relevant to future source-load variation. Third, the forecasting results are directly incorporated into a rolling optimization model for hybrid energy storage dispatch, forming a closed-loop mechanism between prediction and control. Fourth, the battery and supercapacitor are coordinated according to their complementary characteristics: the battery is mainly used for low-frequency energy balancing, while the supercapacitor suppresses high-frequency power fluctuation, thereby reducing battery regulation burden and improving grid-connected power smoothing capability.

The proposed method establishes a unified optimization process by jointly considering source-load forecasts, battery state of charge, supercapacitor state of charge, electricity price signals, power balance constraints, storage operation limits, and grid ramping constraints. The optimization objective includes grid purchase cost, storage degradation cost, renewable curtailment penalty, load shedding penalty, and grid power fluctuation penalty. In practical operation, the system only executes the first-step optimal command in each prediction horizon and then updates the forecasting and optimization results at the next dispatch interval. This rolling mechanism enables the system to respond in advance to renewable ramping, sudden photovoltaic drops, and load peak variations. Experiments are conducted from the perspectives of forecasting accuracy, dispatch economy, power smoothing, renewable energy accommodation, multi-scenario robustness, and parameter sensitivity, verifying the effectiveness and adaptability of the proposed method under high renewable fluctuation, increased load peak-valley difference, forecasting error perturbation, and limited energy storage capacity scenarios.

2. System Architecture and Problem Description

2.1. Smart Grid Structure with Renewable Energy and Hybrid Energy Storage

The studied system is a local smart grid consisting of wind power generation, photovoltaic generation, local loads, a public grid interface, and a battery–supercapacitor hybrid energy storage system, as shown in Fig. 1. Renewable generation is prioritized to supply local loads. When renewable generation exceeds load demand, the surplus power can be stored in the hybrid energy storage system or exchanged with the public grid under grid-connected constraints. When renewable generation is insufficient, the power deficit is compensated by battery discharging, supercapacitor discharging, or grid purchase. This structure is consistent with typical microgrid energy management systems, in which distributed generation, storage units, loads, and the utility grid must be coordinated to ensure stable and economical operation [16].

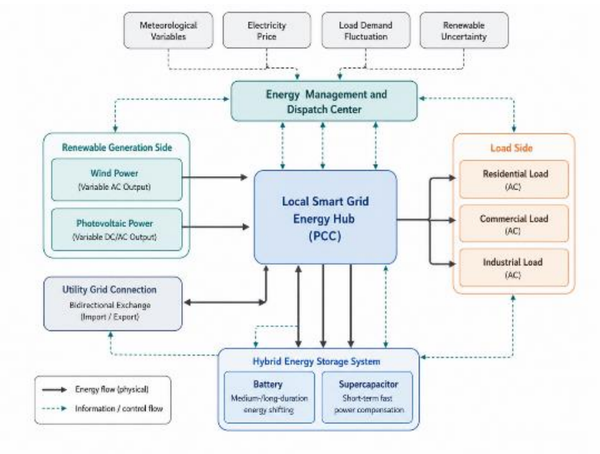

Figure 1. Energy management architecture of a local smart grid with renewable generation and hybrid energy storage

In this system, the hybrid energy storage system consists of a battery and a supercapacitor. The battery has relatively high energy density and is mainly responsible for peak shaving, valley filling, cross-period energy balancing, and surplus renewable energy absorption. The supercapacitor has relatively high power density and fast response capability, and is mainly used to buffer short-term power shocks and suppress high-frequency fluctuations. Existing studies have shown that different energy storage technologies differ significantly in power response speed, energy capacity, efficiency, lifetime, and cost. A single storage technology is difficult to simultaneously meet the requirements of long-duration energy support and short-term power smoothing. Therefore, a battery–supercapacitor hybrid energy storage system can provide complementarity between energy-type and power-type storage, helping to reduce battery degradation caused by frequent charging and discharging while improving the dynamic response capability of the system to renewable energy fluctuations and sudden load changes. The energy management system collects renewable energy output, load demand, meteorological information, electricity price signals, and energy storage states, and then sends these data to the forecasting and optimization dispatch modules. The forecasting module predicts the future renewable generation and load trajectories, while the optimization module generates charging and discharging commands for the battery and supercapacitor according to the predicted source-load states and the current state of charge. The system power balance relationship can be expressed as follows:

$$P_{grid,t} + P_{ren,t} + P_{bat,t} + P_{sc,t} + P_{loss,t} = P_{load,t} + P_{cur,t} \tag{1}$$

where, $P_{grid,t}$ denotes the grid interaction power, $P_{ren,t}$ denotes the total output power of wind power and photovoltaic generation, $P_{bat,t}$ denotes the battery power, $P_{sc,t}$ denotes the supercapacitor power, $P_{loss,t}$ denotes the load shedding power, $P_{load,t}$ denotes the load demand, $P_{cur,t}$ denotes the wind and solar curtailment power. In this paper, energy storage discharging is defined as positive, while charging is defined as negative.

2.2. Modeling of Renewable Energy Generation and Load Uncertainty

The uncertainty of renewable energy generation mainly originates from variations in meteorological conditions. Wind power is affected by wind speed, wind direction, air density, and the operating state of wind turbines. Photovoltaic power is influenced by solar irradiance, temperature, cloud cover, and the day-night cycle. Load uncertainty is closely related to user behavior, weekday type, seasonal variation, meteorological conditions, and electricity pricing mechanisms [17]. These factors do not act independently. For example, solar irradiance and temperature affect photovoltaic output, while temperature and time-of-use price may also affect user load demand. Therefore, a joint source-load modeling strategy is required to describe the coupled evolution of renewable generation and load demand.

To characterize source-load uncertainty, this paper constructs a multi-source input feature vector that includes renewable generation, load power, meteorological variables, electricity price, and periodic time information:

$$\mathbf{x}_t = [P_{w,t}, P_{pv,t}, P_{load,t}, T_t, H_t, V_t, G_t, \lambda_t, C_t] \tag{2}$$

where, $P_{w,t}$ denotes wind power, $P_{pv,t}$ denotes photovoltaic power, $P_{load,t}$ denotes load power, T_t、H_t、V_t、G_t represent temperature, humidity, wind speed, and solar irradiance, respectively, λ_t denotes the time-of-use electricity price, C_t denotes the temporal encoding feature. Given a historical window length L, the input sequence is defined as:

$$\mathbf{X}_{t-L+1:t} = [\mathbf{x}_{t-L+1}, \mathbf{x}_{t-L+2}, \dots, \mathbf{x}_t] \in \mathbb{R}^{L\times d} \quad (3)$$

The objective of the model is to predict renewable energy generation and load demand over the next T time steps:

$$[\hat{P}_{ren,t+1:t+T}, \hat{P}_{load,t+1:t+T}] = f_\theta(\mathbf{X}_{t-L+1:t}) \quad (4)$$

Where $\hat{P}_{ren,t+1:t+T}$ denotes the predicted renewable energy output sequence $\hat{P}_{load,t+1:t+T}$ denotes the predicted load demand sequence.

By predicting renewable generation and load demand within the same model, the proposed method can learn shared temporal representations from source-side and load-side variables. The obtained forecasting results are then directly used as inputs of the rolling optimization dispatch model, enabling the hybrid energy storage system to respond in advance to future net load changes.

3. Prediction-Driven CNN-Attention Source-Load and Hybrid Energy Storage Coordinated Optimization Model

The proposed model does not simply connect renewable energy generation forecasting, load forecasting, and hybrid energy storage optimization dispatch in a sequential manner. Instead, it constructs a prediction-driven source-load and energy storage coordinated optimization framework. Taking multi-source temporal data as input, the framework uses the convolutional neural network-attention (CNN-Attention) model to extract the coupling relationships among renewable energy output, load demand, meteorological factors, electricity prices, and temporal labels, thereby obtaining source-load forecasting results within the future dispatch horizon [18,19]. Subsequently, the forecasting results are directly fed into the hybrid energy storage coordinated optimization module[20,21]. By considering the operating states of the battery and supercapacitor, grid interaction power constraints, and economic objectives, the module generates charging and discharging commands for the energy storage system [22,23]. The overall structure of the model is shown in Fig. 2.

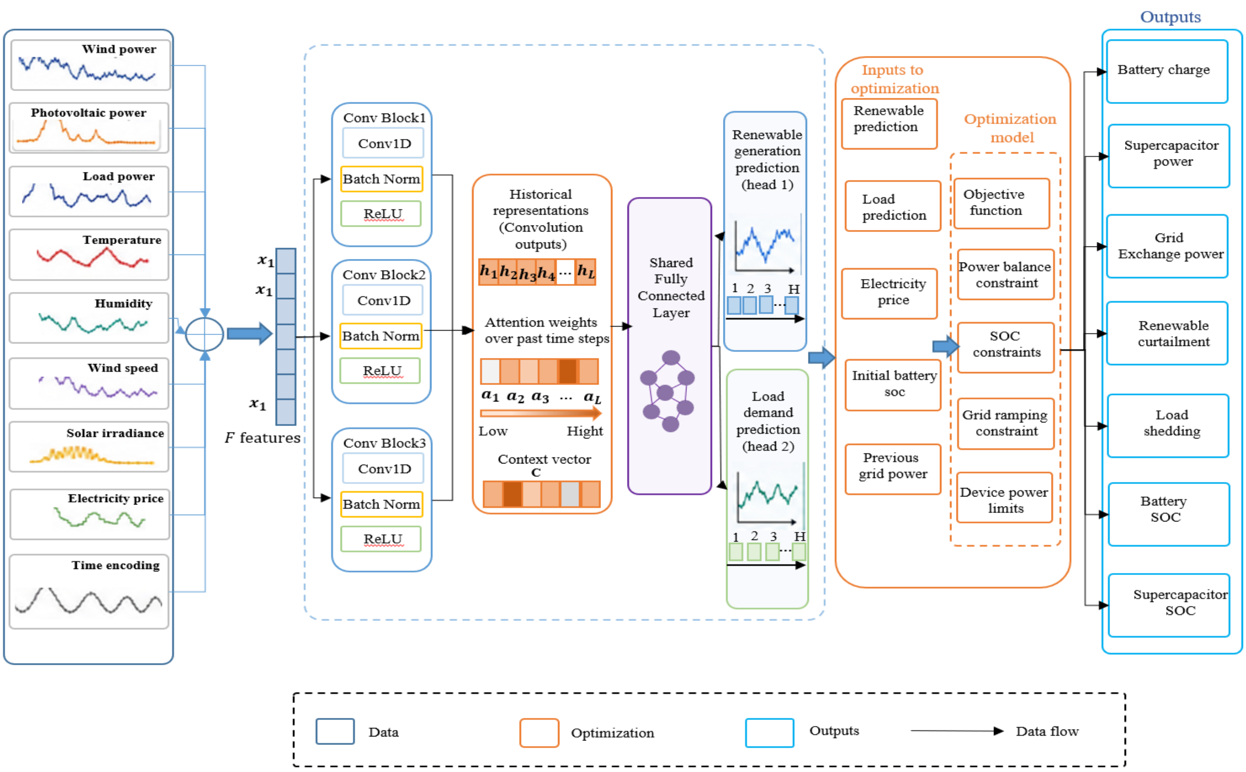

Figure 2. Overall framework of the prediction-driven CNN-Attention source-load and hybrid energy storage coordinated optimization model

In this framework, the CNN-Attention module realizes joint source-load forecasting, while the hybrid energy storage module generates scheduling decisions. The two modules are closely coupled through the prediction horizon, state of charge (SOC), power balance constraints, and grid interaction constraints. This coupling enables the system to reduce operation cost, improve renewable energy accommodation, and stabilize grid-connected power [24,25]. Different from separate forecasting or independent energy storage optimization methods, the proposed model takes predicted source-load trajectories as direct optimization inputs, enabling the energy storage system [26] to respond in advance to future source-load changes and strengthening the adaptability of the system to renewable energy and load fluctuations [27,28].

3.1. Overall Model Framework

Assume that, at time t, the smart grid collects multi-source operational data from the past L time steps, including wind power, photovoltaic power, load power, meteorological variables, electricity price signals, and temporal labels. The model first constructs the historical input sequence as follows:

$$\mathbf{X}_{t-L+1:t} = [\mathbf{x}_{t-L+1}, \mathbf{x}_{t-L+2}, \ldots, \mathbf{x}_t] \in \mathbb{R}^{L\times d} \quad (5)$$

where L denotes the length of the historical input window, and d denotes the input feature dimension. Based on this input sequence, the CNN-Attention model predicts renewable energy generation and load demand over the next T dispatch periods:

$$[\hat{P}_{ren,t+1:t+T}, \hat{P}_{load,t+1:t+T}] = f_\theta(\mathbf{X}_{t-L+1:t}) \quad (6)$$

where, $\hat{P}_{ren,t+1:t+T}$ denotes the predicted total renewable energy output over the future horizon, $\hat{P}_{load,t+1:t+T}$ denotes the predicted load demand, $f_\theta(\mathbf{X}_{t-L+1:t})$ represents the CNN-Attention-based joint source-load forecasting function.

After obtaining the forecasting results, the hybrid energy storage optimization module takes the current battery SOC, supercapacitor SOC, and time-of-use electricity price as inputs, and solves the charging and discharging power of the energy storage system over the next T time steps:

$$[P_{bat,t:t+T}, P_{sc,t:t+T}, P_{grid,t:t+T}] = g_\phi(\hat{P}_{ren}, \hat{P}_{load}, SOC_{bat,t}, SOC_{sc,t}, \lambda_t) \quad (7)$$

where, P_{bat} denotes the battery power, P_{sc} denotes the supercapacitor power, P_{grid} denotes the grid interaction power, $g_\phi(\cdot)$represents the prediction-driven hybrid energy storage optimization dispatch function. In practical operation, the system only executes the optimal control command at the current time step, and then performs forecasting and optimization again at the next dispatch interval.

3.2. Construction of Multi-Source Temporal Features

Renewable energy generation and load demand both exhibit multivariate, strongly temporal, and nonlinear coupling characteristics. Wind power is mainly affected by wind speed, wind direction, and air density; photovoltaic power is mainly influenced by solar irradiance, temperature, and the diurnal cycle; and load power is jointly affected by user behavior, meteorological conditions, weekday type, and electricity pricing mechanisms [29,30]. In practical smart grid operation, these variables are not independent from each other. For example, solar irradiance and temperature directly influence photovoltaic output, while temperature and time-of-use electricity price may also affect user load demand [31,32]. Therefore, the model needs to construct multi-source temporal features to describe the dynamic coupling relationship between renewable generation and load demand.

To enhance the model's ability to characterize source-load uncertainty, this paper constructs the following multi-source input features:

$$\mathbf{x}_t = [P_{w,t}, P_{pv,t}, P_{load,t}, T_t, H_t, V_t, G_t, \lambda_t, C_t] \quad (8)$$

where, $P_{w,t}$ denotes wind power, $P_{pv,t}$ denotes photovoltaic power, $P_{load,t}$ denotes load power., T_t、H_t、V_t、G_t denote temperature, humidity, wind speed, and solar irradiance, respectively, λ_t denotes the time-of-use electricity price, C_t denotes the temporal encoding feature. To avoid destroying the periodic relationships of temporal variables through discrete encoding, this paper adopts sine and cosine encoding for periodic features such as hour, weekday, and month. Taking the hour variable as an example:

$$h_{sin} = \sin\left(\frac{2\pi h}{24}\right) h_{cos} = \cos\left(\frac{2\pi h}{24}\right) \quad (9)$$

where h denotes the current hour. After missing-value processing, outlier correction, and normalization, sliding windows are used to construct the input samples for the model.

3.3. CNN-Attention Joint Source-Load Forecasting Module

The CNN-Attention joint source-load forecasting module is shown in Fig. 3, namely the CNN-Attention joint source-load forecasting and attention-weighted structure. This module consists of a one-dimensional convolutional feature extraction layer, a temporal attention layer, a shared feature layer, and a dual-task output layer.

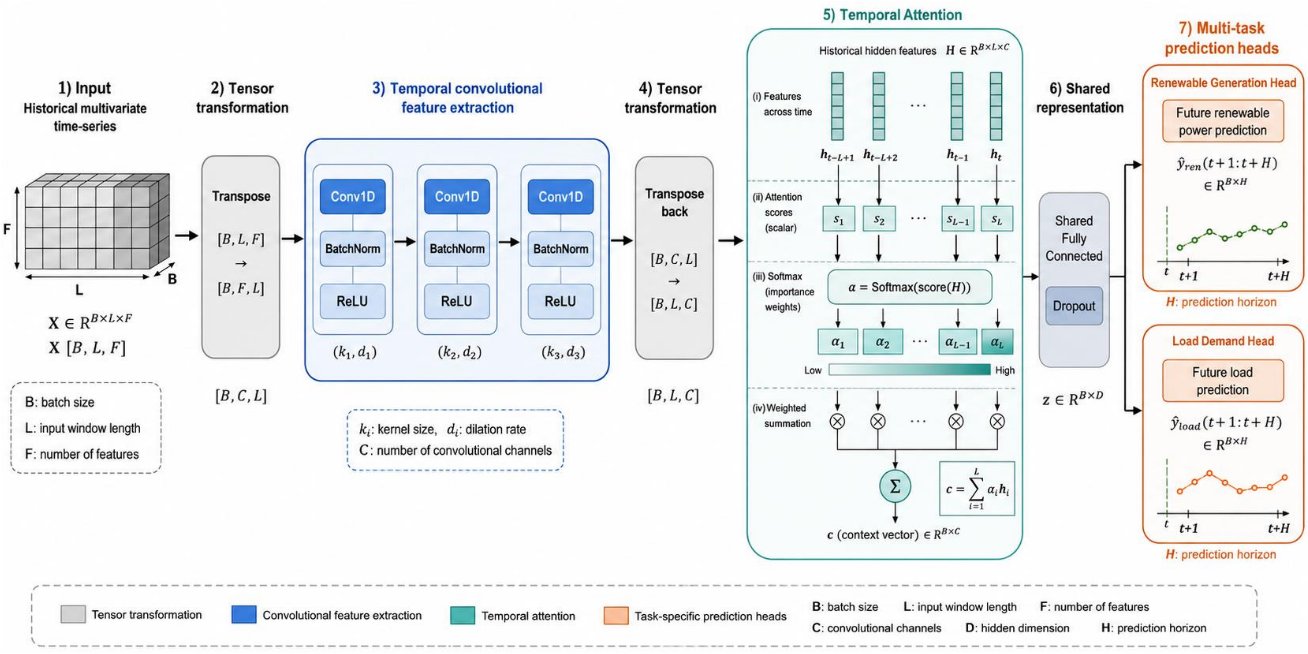

Figure 3. CNN-Attention joint source-load forecasting and attention-weighted structure

The one-dimensional CNN is used to extract local fluctuation patterns from the source-load sequence. For the input sequence X, the convolution output can be expressed as:

$$\mathbf{F}_k = \sigma(\mathbf{W}_k * \mathbf{X} + \mathbf{b}_k) \quad (10)$$

where, $\mathbf{W}_k$ denotes the k-th convolution kernel, $\mathbf{b}_k$ is the bias term, $*$ represents the one-dimensional convolution operation, and $\sigma(\cdot)$denotes the nonlinear activation function. After multiple convolutional layers, the temporal feature map is obtained as:

$$\mathbf{F} = [\mathbf{f}_1, \mathbf{f}_2, \ldots, \mathbf{f}_L] \in \mathbb{R}^{L\times C} \quad (11)$$

where C denotes the number of convolution output channels. This feature map preserves the local variation information of different historical time slices. In renewable energy and load forecasting, different historical time slices contribute differently to future power variations. Therefore, this paper introduces a temporal attention mechanism to adaptively weight the temporal features extracted by the CNN. The attention score of the i-th time slice is defined as:

$$e_i = \mathbf{v}^T \tanh(\mathbf{W}_a \mathbf{f}_i + \mathbf{b}_a) \quad (12)$$

The corresponding attention weight is:

$$\alpha_i = \frac{\exp(e_i)}{\sum_{j=1}^{L} \exp(e_j)} \quad (13)$$

The weighted global temporal representation is then obtained as:

$$\mathbf{z} = \sum_{i=1}^{L} \alpha_i \mathbf{f}_i \quad (14)$$

where α_i denotes the contribution degree of the i-th historical time slice to the forecasting result. Through this mechanism, the model can automatically focus on more critical historical information before wind power fluctuations, photovoltaic ramping, and load peaks occur.

At the output end, this paper adopts a shared feature layer and dual-task prediction heads. The shared layer is used to learn common features between renewable energy output and load variation, while the two prediction heads output renewable power and load power, respectively:

$$\hat{P}_{ren} = \mathbf{W}_{ren}\mathbf{z} + \mathbf{b}_{ren} \quad (15)$$

$$\hat{P}_{load} = \mathbf{W}_{load}\mathbf{z} + \mathbf{b}_{load} \quad (16)$$

The joint forecasting loss function is defined as:

$$\mathcal{L}_{pre} = \beta_1 \frac{1}{T}\sum_{i=1}^{T} |\hat{P}_{ren,t+i} - P_{ren,t+i}| + \beta_2 \frac{1}{T}\sum_{i=1}^{T} |\hat{P}_{load,t+i} - P_{load,t+i}| + \beta_3 \mathcal{L}_{smooth} \quad (17)$$

where β_1, β_2, and β_3 are the loss weights for renewable energy forecasting, load forecasting, and the smoothing term, respectively. $\mathcal{L}_{smooth}$ is used to reduce non-physical abrupt changes in short-term prediction curves. The three weights were selected according to validation-set performance. Since renewable generation forecasting and load forecasting are both directly related to subsequent dispatch decisions, β_1 and β_2 were assigned comparable weights. The smoothing term was used as a regularization term, so β_3 was set to a smaller value. In the experiments, the final values were set to (β_1=0.45), (β_2=0.45), and (β_3=0.10).

3.4. State Modeling of the Battery–Supercapacitor Hybrid Energy Storage System

Based on the forecasting results, the model further performs state modeling for the battery–supercapacitor hybrid energy storage system. The battery has a relatively high energy density and is suitable for low-frequency energy balancing tasks. The supercapacitor has a relatively high power density and fast response speed, making it suitable for suppressing high-frequency power fluctuations. The coordinated operation of the two can reduce lifetime degradation caused by frequent charging and discharging of a single battery system, while enhancing the system's response capability to short-term power shocks. The battery SOC update equation is:

$$SOC_{bat,t+1} = SOC_{bat,t} - \frac{P_{bat,t}\Delta t}{\eta_{bat}E_{bat}} \quad (18)$$

The supercapacitor SOC update equation is:

$$SOC_{sc,t+1} = SOC_{sc,t} - \frac{P_{sc,t}\Delta t}{\eta_{sc}E_{sc}} \quad (19)$$

where, $SOC_{bat,t}$ and $SOC_{sc,t}$ denote the states of charge of the battery and supercapacitor at time t, respectively, E_{bat} and E_{sc} denote their rated capacities, η_{bat} and η_{sc} denote their charging/discharging efficiencies, Δt denotes the dispatch time interval. To more accurately describe the charging and discharging process of energy storage, the charging efficiency and discharging efficiency can also be modeled separately. When $P_{bat,t} < 0$ the battery is charging, while $P_{bat,t} > 0$ indicates battery discharging. The same sign convention is used for the supercapacitor power.

3.5. Source-Load Forecasting-Driven Coordinated Optimization Objective Function

The hybrid energy storage optimization module takes the renewable energy output prediction and load prediction produced by the CNN-Attention model as inputs. Its objective is to minimize the comprehensive operating cost of the system while satisfying power balance and equipment constraints. The optimization objective includes grid purchase cost, energy storage degradation cost, renewable energy curtailment penalty, load shedding penalty, and grid-connected power fluctuation penalty: :

$$minJ = C_{grid} + C_{deg} + C_{cur} + C_{loss} + C_{fluc} \quad (20)$$

where the grid purchase cost is:

$$C_{grid} = \sum_{t=1}^{T} \lambda_t max(P_{grid,t}, 0)\Delta t \quad (21)$$

The energy storage degradation cost is:

$$C_{deg} = \sum_{t=1}^{T} (c_{bat}|P_{bat,t}| + c_{sc}|P_{sc,t}|)\Delta t \quad (22)$$

The renewable energy curtailment penalty is:

$$C_{cur} = \sum_{t=1}^{T} c_{cur}P_{cur,t}\Delta t \quad (23)$$

The load shedding penalty is:

$$C_{loss} = \sum_{t=1}^{T} c_{loss}P_{loss,t}\Delta t \quad (24)$$

The grid-connected power fluctuation penalty is:

$$C_{fluc} = \sum_{t=2}^{T} c_{fluc}(P_{grid,t} - P_{grid,t-1})^2 \quad (25)$$

This objective function directly couples the forecasting results with energy storage dispatch, enabling the model to adjust the operating states of the energy storage system in advance according to the future trends of renewable energy output and load variation.

3.6. Grid Stability and Energy Storage Operation Constraints

Within the dispatch horizon, the system must satisfy the power balance constraint:

$$P_{grid,t} + \hat{P}_{ren,t} + P_{bat,t} + P_{sc,t} + P_{loss,t} = \hat{P}_{load,t} + P_{cur,t} \quad (26)$$

where, $\hat{P}_{ren,t}$ and $\hat{P}_{load,t}$ denote the renewable energy output and load demand predicted by the CNN-Attention model, respectively.

The battery power constraint is:

$$-P_{bat}^{ch,max} \leq P_{bat,t} \leq P_{bat}^{dis,max} \quad (27)$$

The supercapacitor power constraint is:

$$-P_{sc}^{ch,max} \leq P_{sc,t} \leq P_{sc}^{dis,max} \quad (28)$$

The battery SOC constraint is:

$$SOC_{bat}^{min} \leq SOC_{bat,t} \leq SOC_{bat}^{max} \quad (29)$$

The supercapacitor SOC constraint is:

$$SOC_{sc}^{min} \leq SOC_{sc,t} \leq SOC_{sc}^{max} \quad (30)$$

The grid interaction power constraint is:

$$P_{grid}^{min} \leq P_{grid,t} \leq P_{grid}^{max} \quad (31)$$

The grid-connected power ramping constraint is:

$$|P_{grid,t} - P_{grid,t-1}| \leq R_{grid}^{max} \quad (32)$$

Renewable energy curtailment and load shedding satisfy the following non-negativity constraints:

$$P_{cur,t} \geq 0, P_{loss,t} \geq 0 \quad (33)$$

The above constraints jointly ensure the safe operation of energy storage devices, smooth variation of grid interaction power, and dispatch results within the physical boundaries of the equipment.

To reduce the influence of forecasting error accumulation on dispatch results, this paper adopts a prediction-driven rolling optimization strategy. At each dispatch time, the system first collects multi-source operational data from the most recent L time steps and inputs them into the CNN-Attention model to obtain renewable energy output and load demand predictions over the next T time steps. Then, the optimization module solves the energy storage dispatch scheme over the entire prediction horizon based on the predicted values, current SOC, electricity price signals, and grid constraints. The system only executes the current optimal battery power $P_{bat,t}^{*}$ and supercapacitor power $P_{sc,t}^{*}$, At the next time step, new data are collected, and the forecasting and optimization results are updated again. The rolling optimization process can be expressed as follows:

$$[\hat{P}_{ren,t+1:t+T}, \hat{P}_{load,t+1:t+T}] = f_\theta(\mathbf{X}_{t-L+1:t}) \quad (34)$$

$$[P_{bat,t:t+T}^{*}, P_{sc,t:t+T}^{*}, P_{grid,t:t+T}^{*}] = g_\phi(\hat{P}_{ren}, \hat{P}_{load}, SOC_{bat,t}, SOC_{sc,t}, \lambda_t) \quad (35)$$

This strategy forms a closed loop between forecasting and dispatch: the forecasting module provides future source-load states for the optimization module, while the execution results of the optimization module further affect the energy storage SOC and system operating state at the next time step. Compared with fixed day-ahead dispatch, rolling optimization can correct forecasting deviations more promptly and improve the system's adaptability to renewable energy fluctuations and load variations.

4. Experimental Design

4.1. Dataset and Preprocessing

Experiments were conducted using anonymized operational data from a regional wind–photovoltaic–storage microgrid from January 1, 2023 to December 31, 2023. The dataset includes wind power, photovoltaic power, load demand, meteorological variables, time-of-use electricity price, and hybrid energy storage information, with a 15-min sampling interval and 35,040 time steps. The studied system consists of a 300 kW wind unit, a 500 kW photovoltaic unit, a 540 kWh battery, and a 35 kWh supercapacitor. The load demand ranges from approximately 610 kW to 1180 kW, with an average of 923 kW, while renewable generation ranges from 0 kW to 720 kW, with an average of 204 kW.

The data were chronologically divided into training, validation, and test sets at ratios of 70%, 15%, and 15%. Missing values were filled by linear interpolation, abnormal values were corrected using adjacent mean values, and Z-score normalization was applied to power and meteorological variables. Sine-cosine encoding was used for periodic time features to preserve temporal periodicity. The main characteristics of the dataset and the microgrid configuration are summarized in Table 1.

Table 1. Dataset statistics

Item	Value
Data source	Anonymized operational data of a regional wind–photovoltaic–storage microgrid
Time span	2023.01.01–2023.12.31
Sampling interval	15 min
Number of samples	35,040
Wind generation capacity	300 kW
Photovoltaic generation capacity	500 kW
Battery capacity	540 kWh
Supercapacitor capacity	35 kWh
Renewable generation range	0–720 kW
Average renewable generation	204 kW
Load demand range	610–1180 kW
Average load demand	923 kW
Number of input features	12
Training/validation/test split	70% / 15% / 15%

The input features include wind power, photovoltaic power, load power, temperature, humidity, wind speed, solar irradiance, time-of-use electricity price, hour sine encoding, hour cosine encoding, weekday sine encoding, and weekday cosine encoding, giving a total of 12 features.

4.2. Comparative Methods

To ensure the fairness of comparison, all forecasting models were trained using the same training, validation, and test sets. The optimizer, learning rate, batch size, weight decay, dropout, input window length, prediction horizon, and number of epochs were kept consistent. For each baseline model, the main hidden dimension was set to 128, and the model depth was controlled within a comparable range. Hyperparameters were selected according to validation-set performance, and the model with the lowest validation error was used for testing.

4.3. Experimental Environment and Parameter Settings

All experiments were implemented in Python 3.9. The forecasting models were developed using PyTorch, and data processing was supported by NumPy, Pandas, and Scikit-learn. The rolling optimization problem was solved using the SLSQP algorithm in SciPy. Model training and testing were conducted on a workstation equipped with an Intel Core i7-12700K CPU, 32 GB RAM, and an NVIDIA GeForce RTX 3060 GPU with 12 GB video memory. The operating system was Windows 11, and CUDA 11.8 was used for GPU acceleration. For fair comparison, all models used the same dataset split and training settings. Given the 15-min sampling interval, the input window length was set to 96, corresponding to 24 h of historical data, and the prediction horizon was set to 16, corresponding to 4 h ahead forecasting. The 4 h window was selected to balance short-term renewable/load variation coverage, forecasting reliability, and the charging–discharging response characteristics of the battery–supercapacitor hybrid energy storage system. Other training settings are listed in Table 2.

Table 2. Model training parameter settings

Parameter	Value
Input window length ((L))	96
Prediction horizon ((T))	16
CNN kernel size	3
Number of CNN channels	64
Hidden layer dimension	128
Dropout	0.2
Batch size	64
Optimizer	AdamW

Learning rate	0.001
Weight decay	0.0001
Epochs	100
Loss function	Smooth L1 Loss

4.4. Evaluation Metrics

The forecasting accuracy is evaluated using MAE, RMSE, and MAPE:

$$MAE = \frac{1}{N}\sum_{i=1}^{N} |\hat{y}_i - y_i| \quad (36)$$

$$RMSE = \sqrt{\frac{1}{N}\sum_{i=1}^{N} (\hat{y}_i - y_i)^2} \quad (37)$$

$$MAPE = \frac{1}{N}\sum_{i=1}^{N} \left|\frac{\hat{y}_i - y_i}{y_i}\right| \times 100\% \quad (38)$$

where, $\hat{y}_i$ denotes the predicted value, y_i denotes the true value, N denotes the number of test samples. MAE and RMSE are used to measure the absolute level of prediction error, while MAPE is used to measure the relative error. The dispatch performance is evaluated using comprehensive operating cost, renewable energy accommodation rate, wind and solar curtailment rate, load shedding rate, grid-connected power fluctuation rate, and battery equivalent cycle number. The renewable energy accommodation rate is defined as:

$$R_{ren} = \frac{\sum P_{ren,t}^{use}}{\sum P_{ren,t}^{available}} \times 100\% \quad (39)$$

The wind and solar curtailment rate is defined as:

$$R_{cur} = \frac{\sum_{t=1}^{T} P_{cur,t}}{\sum_{t=1}^{T} P_{ren,t}} \times 100\% \quad (40)$$

The load shedding rate is defined as:

$$R_{loss} = \frac{\sum_{t=1}^{T} P_{loss,t}}{\sum_{t=1}^{T} P_{load,t}} \times 100\% \quad (41)$$

The grid-connected power fluctuation rate is defined as:

$$FR = \frac{1}{T-1}\sum_{t=2}^{T} \frac{|P_{grid,t} - P_{grid,t-1}|}{P_{grid}^{rated}} \times 100\% \quad (42)$$

where, $P_{ren,t}$ denotes the total renewable energy output, $P_{cur,t}$ denotes the wind and solar curtailment power, $P_{loss,t}$ denotes the load shedding power, $P_{load,t}$ denotes the load power, $P_{grid,t}$ denotes the grid interaction power.

5. Experimental Results and Analysis

This section analyzes the experimental results from the perspectives of renewable energy and load forecasting performance, coordinated dispatch performance of hybrid energy storage, grid-connected power smoothing capability, system economy, renewable energy accommodation capability, multi-scenario robustness, and parameter sensitivity. To enhance the systematic presentation of the results, the relevant results are integrated into multi-subfigure formats, so that forecasting performance, dispatch behavior, and comprehensive operating effects can be compared from a unified perspective.

5.1. Forecasting Performance Analysis

This section mainly verifies the performance of different forecasting models in renewable energy output and load power forecasting tasks. To simultaneously present the curve tracking capability and error distribution characteristics of the models, this paper integrates the renewable energy forecasting curves, load forecasting curves, and the two types of forecasting error distributions into Fig. 4.

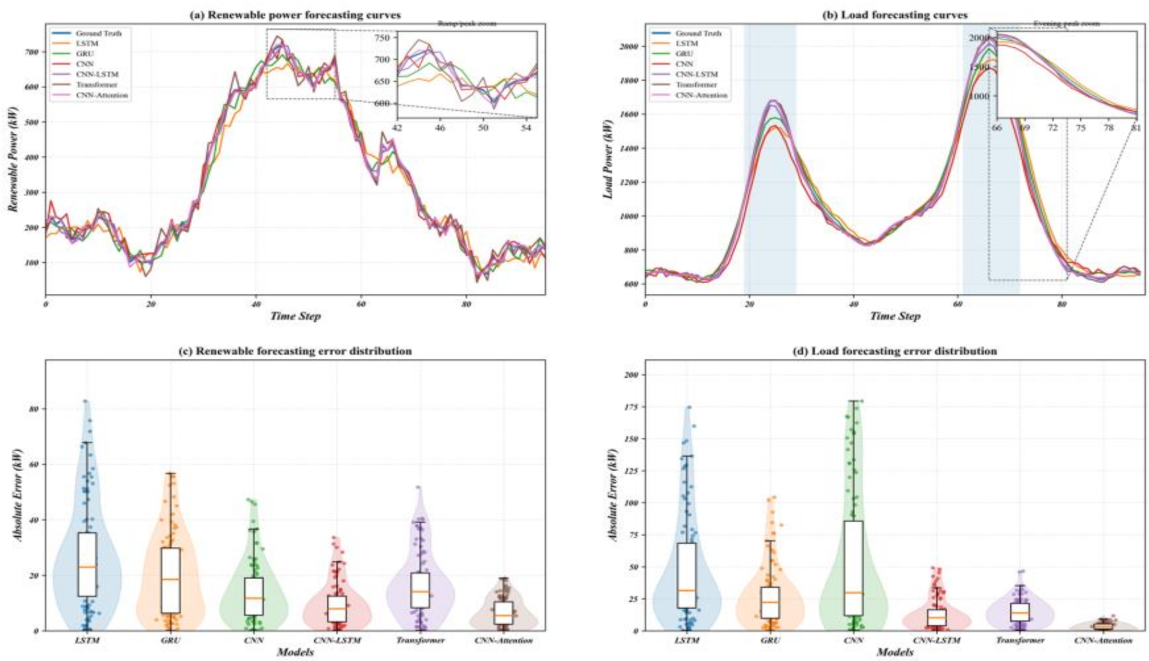

Figure 4. Forecasting performance comparison of different models

(a) Renewable power forecasting curves; (b) load forecasting curves; (c) renewable forecasting error distribution; (d) load forecasting error distribution.

Fig.4 compares source-load forecasting results of various models, including renewable energy output, load prediction curves and error distributions. For renewable energy forecasting, LSTM and GRU lag in rapid power fluctuation periods, CNN deviates in long-term trends, and Transformer has local prediction oscillations. In contrast, CNN-Attention fits actual data best with the lowest errors (MAE=6.6917 kW, RMSE=8.3218 kW, MAPE=3.2881%), as listed in Table 3. In load forecasting, all models perform steadily in normal periods but differ greatly at load peaks. Most existing models show peak response delay, value underestimation or obvious fluctuations. CNN-Attention outperforms others in peak tracking, with forecasting errors of 3.7473 kW (MAE), 4.4898 kW (RMSE) and 0.4060% (MAPE), as shown in Table 4. Its error distribution is the most concentrated with superior stability. Combining CNN local feature extraction and attention-based key time-series adaptive weighting, CNN-Attention obtains optimal source-load forecasting accuracy, offering solid data support for hybrid energy storage optimal dispatch.

Table 3. Renewable energy output forecasting performance of different forecasting models

Method	MAE/kW	RMSE/kW	MAPE/%
LSTM	26.575	32.721	11.267
GRU	19.752	24.701	8.506
CNN	13.781	17.661	6.616
CNN-LSTM	9.496	12.213	4.738
Transformer	16.243	19.878	7.640
CNN-Attention	6.692	8.322	3.288

Table 4. Load forecasting performance of different forecasting models

Method	**MAE/kW**	**RMSE/kW**	**MAPE/%**
LSTM	13.286	16.742	1.431
GRU	10.574	13.218	1.137
CNN	7.426	9.386	0.803
CNN-LSTM	5.284	6.515	0.586
Transformer	6.917	8.604	0.746
CNN-Attention	3.747	4.490	0.406

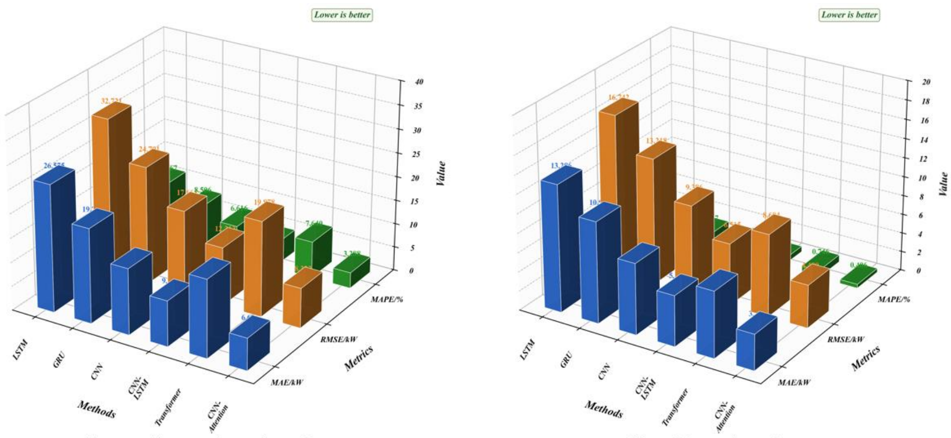

(a) Renewable power forecasting performance (b) Load forecasting performance

Figure 5. Forecasting performance comparison of different models for renewable generation and load prediction

Fig. 5 compares the forecasting performance of different models using MAE, RMSE, and MAPE. For renewable energy forecasting, LSTM and GRU show relatively large errors, CNN has limited ability to capture long-term dependencies, and Transformer may produce deviations under large fluctuations. CNN-Attention achieves the best performance, with MAE, RMSE, and MAPE of 6.692 kW, 8.322 kW, and 3.288%, respectively. For load forecasting, CNN-Attention also obtains the lowest errors, with MAE, RMSE, and MAPE of 3.747 kW, 4.490 kW, and 0.406%, respectively. These results indicate that combining CNN-based local fluctuation extraction with attention-based key temporal information modeling improves the accuracy and stability of joint source-load forecasting.

To further analyze interpretability, Fig. 6 visualizes the temporal attention weights of CNN-Attention. The model assigns higher weights to key historical time slices before load peaks and rapid photovoltaic variations, indicating that the attention mechanism can capture informative periods related to future source-load changes.

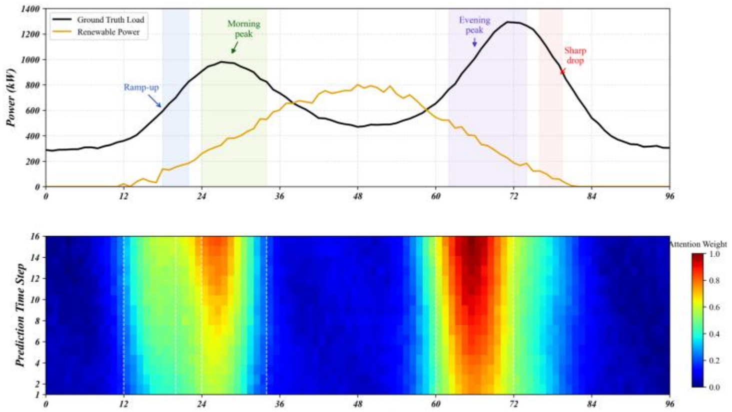

Figure 6. Visualization of CNN-Attention attention weights

5.2. Hybrid Energy Storage Dispatch Results

Figs. 7 and 8 show the coordinated operation results of the hybrid energy storage system under different dispatch strategies. As shown in Fig. 7(a), the single-battery strategy requires the battery to handle both energy balancing and short-term fluctuation compensation, resulting in frequent power variations. Rule-based control and conventional optimization reduce these variations to some extent, but their battery power profiles still contain obvious short-term fluctuations. In contrast, the proposed method produces a smoother battery power curve, indicating that the battery mainly undertakes low-frequency energy balancing.

Fig. 7(b) shows that the supercapacitor responds rapidly to short-term power variations, compensating for high-frequency source-load fluctuations and forming complementary operation with the battery. As shown in Fig. 8(a), the state of charge trajectories of both storage devices remain within safe operating ranges. Fig. 8(b) further shows that the proposed method achieves the smoothest grid-connected power profile and reduces the grid power fluctuation rate to 3.4%, lower than no storage, single-battery storage, rule-based control, and conventional optimization. These results demonstrate that the proposed coordinated dispatch strategy reduces battery regulation burden and improves grid-connected power stability.

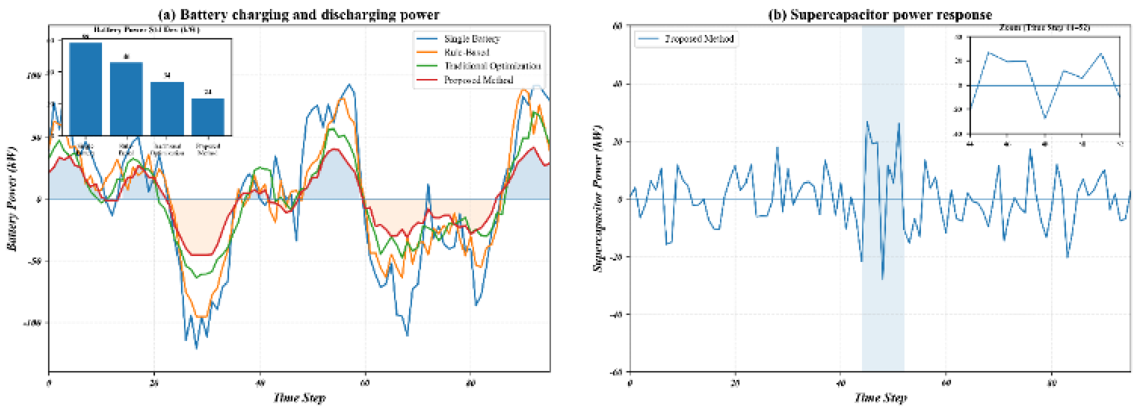

Figure 7. Power response of hybrid energy storage under different dispatch strategies

(a) Battery power comparison; (b) supercapacitor power response

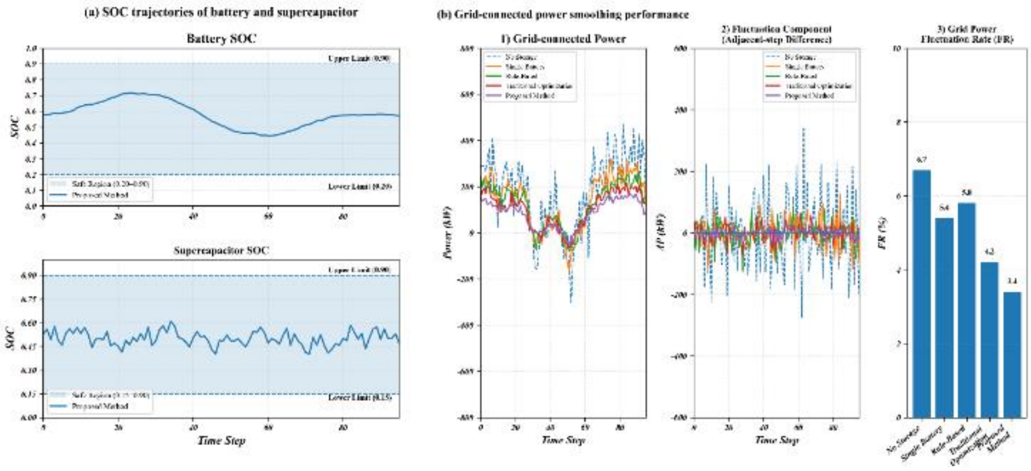

Figure 8. SOC trajectories and grid-connected power smoothing performance of hybrid energy storage

(a) SOC trajectories of the battery and supercapacitor; (b) grid-connected power smoothing effect

5.3. Economic Analysis

Fig. 9 illustrates the components of system operating costs, including grid purchase expense, wind-solar curtailment penalty, energy storage maintenance cost, battery aging cost and load shedding penalty. The no-storage scheme has the highest total cost at 650. Single battery storage and rule-based control cut total costs to 550 and 560 respectively, yet suffer from high battery aging loss and rigid control constraints. Traditional optimization further lowers the total cost to 450 with insufficient hybrid storage coordination.

The proposed method achieves the minimum total operating cost at 360, with prominent cost reduction advantages over other strategies. It effectively curtails grid purchase expenditure, abandonment penalty and load shedding expense. With supercapacitors undertaking high-frequency regulation, battery degradation cost is greatly reduced. The coordinated dispatch strategy significantly improves overall system economic benefits.

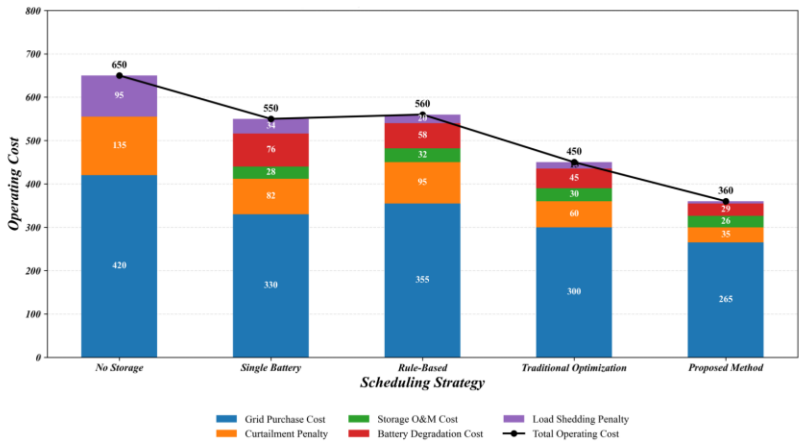

Figure 9. Comparison of system operating cost composition

5.4. Renewable Energy Accommodation Capability Analysis

Fig. 10 presents the renewable energy accommodation rate and wind-solar curtailment rate under different strategies. Without energy storage, the system has the lowest accommodation capacity, reaching an accommodation rate of 65.3% and a curtailment rate of 13.2%. Insufficient regulation leads to severe energy abandonment under high renewable penetration. Single battery storage raises the accommodation rate to 74.1% and cuts the curtailment rate to 8.7%, yet it is restricted in coping with frequent power fluctuations. Rule-based control obtains an accommodation rate of 72.3% and a curtailment rate of 9.6%, showing inferior performance due to poor adaptability to dynamic source-load changes. Traditional optimization further lifts utilization to an accommodation rate of 82.7% and a curtailment rate of 5.6%, while it cannot fully handle short-term power variations and forecast deviations. The proposed strategy achieves the optimal results with an accommodation rate of 90.6% and a curtailment rate of 2.8%. It raises the accommodation rate by 25.3 percentage points and 7.9 percentage points, and reduces the curtailment rate by 10.4 percentage points and 2.8 percentage points compared with the no-storage mode and conventional optimization method respectively. Combining accurate source-load forecasting, this strategy arranges batteries to absorb excess power in advance and adopts supercapacitors to stabilize transient fluctuations, which effectively lowers renewable energy abandonment.

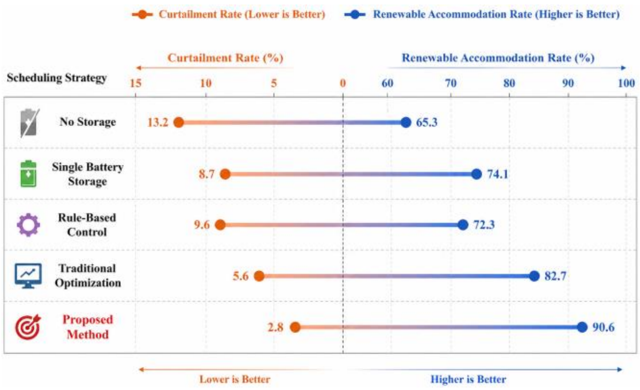

Figure 10. Comparison of renewable energy accommodation rate and wind/solar curtailment rate

5.5. Robustness Analysis Under Different Operating Scenarios

To verify the adaptability of the proposed method, five working scenarios are constructed and assessed via four key indices. Lower operation cost, power fluctuation rate and load shedding rate, together with higher renewable energy accommodation rate, stand for better performance. As shown in Fig.11, the method achieves the best performance under normal conditions, with comprehensive robustness score 0.95. Its robustness declines to 0.74 under intense renewable fluctuations and forecast disturbances, and stays at 0.81 with larger load peak-valley difference. Limited energy storage leads to the lowest score of 0.59. Overall the presented strategy maintains satisfactory operation in most scenarios. Hybrid energy storage coordination and rolling optimization effectively improve system adaptability to source-load uncertainties and forecasting errors.

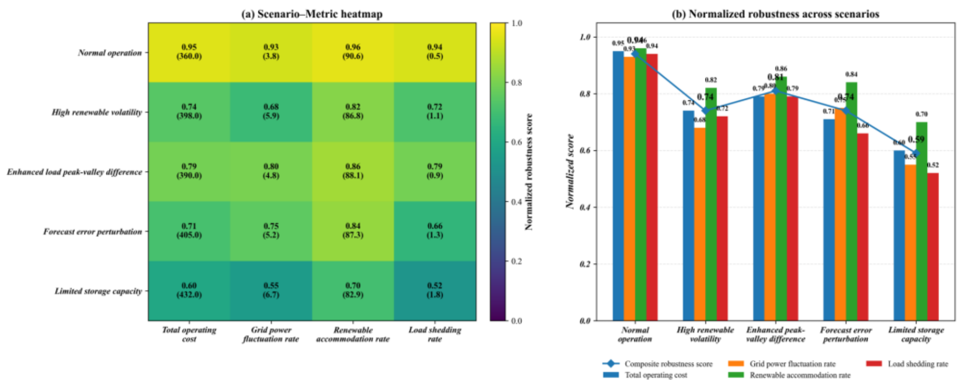

Figure 11. Multi-scenario robustness experimental results

(a) Normalized heatmap of indicators under different operating scenarios; (b) normalized indicator scores and comprehensive robustness scores under different operating scenarios.

5.6 Parameter Sensitivity Analysis

This paper explores how battery and supercapacitor capacities affect system operation cost and grid-connected power fluctuation rate, with results illustrated in Fig.12.Insufficient energy storage leads to high operating costs due to limited power absorption and peak supply capacity. Expanding battery capacity strengthens energy shifting ability and greatly cuts operational expenses. The total cost falls to a low level at battery capacity 540 kWh and supercapacitor capacity 35 kWh. Further capacity expansion brings marginal benefits down and even causes slight cost rise, proving excess storage lacks economic advantages.

Energy storage sizing also remarkably influences power fluctuation level. Small capacity fails to stabilize power variations effectively. Larger batteries improve medium-low frequency power regulation, while larger supercapacitors enhance rapid fluctuation suppression, jointly reducing power fluctuation rate. The minimum fluctuation rate of 0.85% occurs at battery capacity 560 kWh and supercapacitor capacity 30 kWh. Reasonable collocation of the two energy storage devices can effectively optimize grid-connected power smoothing effect.

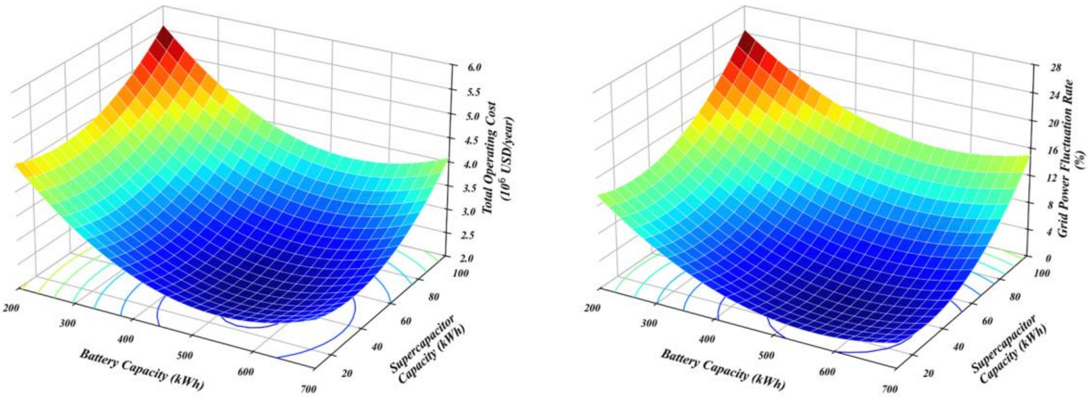

Figure 12. Influence of energy storage capacity on system operating performance

(a) Influence of battery capacity and supercapacitor capacity on the total system operating cost; (b) influence of battery capacity and supercapacitor capacity on the grid-connected power fluctuation rate.

6. Conclusion

This study focuses on source-load uncertainty, severe power fluctuation, and insufficient energy storage dispatch in smart grids with high renewable energy penetration. A CNN-Attention-based source-load forecasting method combined with hybrid energy storage rolling optimization is proposed. The method uses convolutional neural network to extract local fluctuation features and attention mechanism to strengthen key time-series information, and further integrates forecasting results into a prediction-driven rolling dispatch model to form closed-loop operational regulation. The proposed model achieves better forecasting accuracy than the comparison methods. It obtains MAE, RMSE, and MAPE of 6.692 kW, 8.322 kW, and 3.288% for renewable energy forecasting, and 3.747 kW, 4.490 kW, and 0.406% for load forecasting, respectively. These results show that the proposed method improves the tracking ability of renewable power fluctuations and load variations.

In dispatch operation, the hybrid energy storage coordinated strategy reduces the total operating cost to 360 and decreases the grid-connected power fluctuation rate to 3.4%. The battery mainly undertakes low-frequency energy balancing, while the supercapacitor suppresses high-frequency power fluctuations, improving grid power stability. The renewable energy accommodation rate reaches 90.6%, and the curtailment rate decreases to 2.8%. Under multiple operating scenarios, the proposed rolling optimization strategy maintains stable performance, indicating its adaptability to source-load disturbances and forecasting errors.

Overall, the integrated forecasting and dispatch strategy realizes multi-objective optimization in cost reduction, renewable energy accommodation, and power fluctuation suppression. Future work will focus on probabilistic prediction, robust optimization, and practical engineering verification.

References

[1] Aslam S, Herodotou H, Mohsin S M, Javaid N, Ashraf N, Aslam S. A survey on deep learning methods for power load and renewable energy forecasting in smart microgrids[J]. Renewable and Sustainable Energy Reviews, 2021, 144: 110992.

[2] Alkhayat G, Mehmood R. A review and taxonomy of wind and solar energy forecasting methods based on deep learning[J]. Energy and AI, 2021, 4: 100060.
[3] Eren Y, Küçükdemiral İ B. A comprehensive review on deep learning approaches for short-term load forecasting[J]. Renewable and Sustainable Energy Reviews, 2024, 189: 114031.
[4] Ahmad N, Ghadi Y Y, Adnan M, Ali M. Load forecasting techniques for power system: Research challenges and survey[J]. IEEE Access, 2022, 10: 71054-71090.
[5] Wazirali R, Yaghoubi E, Abujazar M S S, Ahmad R, Vakili A H. State-of-the-art review on energy and load forecasting in microgrids using artificial neural networks, machine learning, and deep learning techniques[J]. Electric Power Systems Research, 2023, 225: 109792.
[6] Jurado Egas M F, Samper M E, Rosés R E. An improved encoder-decoder-based CNN model for probabilistic short-term load and PV forecasting[J]. Electric Power Systems Research, 2023, 217: 109153.
[7] Hochreiter S, Schmidhuber J. Long short-term memory[J]. Neural Computation, 1997, 9(8): 1735-1780.
[8] Vaswani A, Shazeer N, Parmar N, Uszkoreit J, Jones L, Gomez A N, Kaiser Ł, Polosukhin I. Attention is all you need[C]//Advances in Neural Information Processing Systems. 2017, 30.
[9] Olabi A G, Onumaegbu C, Wilberforce T, Ramadan M, Abdelkareem M A, Al-Alami A H. Critical review of energy storage systems[J]. Energy, 2021, 214: 118987.
[10] Lin X, Zamora R. Controls of hybrid energy storage systems in microgrids: Critical review, case study and future trends[J]. Journal of Energy Storage, 2022, 47: 103884.
[11] Parisio A, Rikos E, Glielmo L. A model predictive control approach to microgrid operation optimization[J]. IEEE Transactions on Control Systems Technology, 2014, 22(5): 1813-1827.
[12] Hu J, Shan Y, Guerrero J M, Ioinovici A, Chan K W, Rodriguez J. Model predictive control of microgrids: An overview[J]. Renewable and Sustainable Energy Reviews, 2021, 136: 110422.
[13] Wang S, Ma C, Gao H, Deng D, Fernandez C, Blaabjerg F. Improved hyperparameter Bayesian optimization-bidirectional long short-term memory optimization for high-precision battery state of charge estimation[J]. Energy, 2025, 328: 136598.
[14] Wang S, Fu Y, Zhang W, Fernandez C, Blaabjerg F. Review on improved neural network algorithms for battery state of energy estimation in smart grids[J]. Renewable and Sustainable Energy Reviews, 2026, 231: 116797.
[15] Wang S, Gao H, Takyi-Aninakwa P, Guerrero J M, Fernandez C, Huang Q. Improved multiple feature-electrochemical thermal coupling modeling of lithium-ion batteries at low-temperature with real-time coefficient correction[J]. Protection and Control of Modern Power Systems, 2024, 9(3): 157-173.
[16] Al-Ismail F S. DC microgrid planning, operation, and control: A comprehensive review[J]. IEEE Access, 2021, 9: 36154-36172.
[17] Hirsch A, Parag Y, Guerrero J. Microgrids: A review of technologies, key drivers, and outstanding issues[J]. Renewable and Sustainable Energy Reviews, 2018, 90: 402-411.
[18] Tobajas J, Garcia-Torres F, Roncero-Sánchez P, Vázquez J, Bellatreche L, Nieto E. Resilience-oriented schedule of microgrids with hybrid energy storage system using model predictive control[J]. Applied Energy, 2022, 306: 118092.
[19] Li S, Zhu J, Dong H, Zhu H, Fan J. A novel rolling optimization strategy considering grid-connected power fluctuations smoothing for renewable energy microgrids[J]. Applied Energy, 2022, 309: 118441.
[20] LeCun Y, Bottou L, Bengio Y, Haffner P. Gradient-based learning applied to document recognition[J]. Proceedings of the IEEE, 1998, 86(11): 2278-2324.
[21] Lim B, Arik S Ö, Loeff N, Pfister T. Temporal fusion transformers for interpretable multi-horizon time series forecasting[J]. International Journal of Forecasting, 2021, 37(4): 1748-1764.
[22] Zhou H, Zhang S, Peng J, Zhang S, Li J, Xiong H, Zhang W. Informer: Beyond efficient transformer for long sequence time-series forecasting[C]//Proceedings of the AAAI Conference on Artificial Intelligence. 2021, 35(12): 11106-11115.
[23] Oreshkin B N, Carpov D, Chapados N, Bengio Y. N-BEATS: Neural basis expansion analysis for interpretable time series forecasting[J]. International Journal of Forecasting, 2020, 36(3): 1187-1204.
[24] Budiman F N, Ramli M A M, Milyani A H, Bouchekara H R E H, Rawa M, Muktiadji R F, Seedahmed M M A. Stochastic optimization for the scheduling of a grid-connected microgrid with a hybrid energy storage system considering multiple uncertainties[J]. Energy Reports, 2022, 8: 7444-7456.
[25] Mohseni S, Brent A C. Probabilistic sizing and scheduling co-optimisation of hybrid battery/super-capacitor energy storage systems in micro-grids[J]. Journal of Energy Storage, 2023, 73: 109172.
[26] Babaei M R, Ghasemi-Marzbali A, Abbasalizadeh S. Control of a combined battery/supercapacitor storage system for DC microgrid application[J]. Journal of Energy Storage, 2024, 96: 112675.
[27] Chekira O, Boujoudar Y, El Moussaoui H, Boharb A, Lamhamdi T, El Markhi H. An improved microgrid energy management system based on hybrid energy storage system using ANN NARMA-L2 controller[J]. Journal of Energy Storage, 2024, 98: 113096.
[28] Gugulothu R, Nagu B, Pullaguram D, Babu B C. Optimal coordinated energy management strategy for standalone solar photovoltaic system with hybrid energy storage[J]. Journal of Energy Storage, 2023, 67: 107628.
[29] Xu C, Chen G. Interpretable transformer-based model for probabilistic short-term forecasting of residential net load[J]. International Journal of Electrical Power & Energy Systems, 2024, 155: 109515.
[30] Fang B, Xu L, Luo Y, Luo Z, Li W. A method for short-term electric load forecasting based on the FMLP-iTransformer model[J]. Energy Reports, 2024, 12: 3405-3411.
[31] Salinas D, Flunkert V, Gasthaus J, Januschowski T. DeepAR: Probabilistic forecasting with autoregressive recurrent networks[J]. International Journal of Forecasting, 2020, 36(3): 1181-1191.
[32] Akhtar S, Shahzad S, Zaheer A, Ullah H S, Kilic H, Gono R, Jasiński M, Leonowicz Z. Short-term load forecasting models: A review of challenges, progress, and the road ahead[J]. Energies, 2023, 16(10): 4060.